energies

MDPI

Article

Analysis and Evaluation of WBG Power Device in High Frequency Induction Heating Application

Kwang-Hyung Cha, Chang-Tae Ju and Rae-Young Kim *

The Department of Electrical and Biomedical Engineering, Hanyang University, Seoul 04763, Korea; kwanghyung45@hanyang.ac.kr (K.-H.C.); oppiu@hanyang.ac.kr (C.-T.J.)
* Correspondence: rykim@hanyang.ac.kr; Tel.: +82-2-2220-2897

Received: 3 September 2020; Accepted: 12 October 2020; Published: 14 October 2020

Abstract: A device suitability analysis is performed herein by comparing the performance of a silicon carbide (SiC) metal-oxide-semiconductor-field-effect transistor (MOSFET) and a gallium nitride (GaN) high-electron mobility transistor (HEMT), which are wide-bandgap (WBG) power semiconductor devices in induction heating (IH) systems. The WBG device presents advantages such as high-speed switching owing to its excellent physical properties, and when it is applied to the IH system, a high output power can be achieved through high-frequency driving. To exploit these advantages effectively, a suitability analysis comparing SiC and GaN with IH systems is required. In this study, SiC MOSFET and GaN HEMT are applied to the general half-bridge series resonant converter topology, and comparisons of the conduction loss, switching loss, reverse conduction loss, and thermal performance considering the characteristics of the device and the system conditions are performed. Accordingly, the device suitability in an IH system is analyzed. To verify the device conformance analysis, a resonant converter prototype with SiC and GaN rated at 650 V is constructed. The analysis is verified by an experimental comparison of power loss and thermal performance.

Keywords: WBG device; induction heating; GaN HEMT; SiC MOSFET; performance comparison; evaluation

1. Introduction

Owing to the physical limitations of Si, power semiconductor devices are increasingly limited in the development of Si-based devices. Accordingly, interest in wide-bandgap (WBG) devices having excellent physical characteristics has recently increased. Representative examples include silicon carbide (SiC) and gallium nitride (GaN), both of which have better physical properties than conventional Si. These WBG devices have a low on-resistance and switching loss at high voltage ratings and are suitable for high-speed switching. High-speed switching is advantageous with regard to power density and cost because it can reduce the size of the system in various applications. Because of these advantages, studies have been conducted to compare the performance of WBG device-based and Si-based systems in various applications [1–11].

In [1], switching loss and conduction loss were analyzed when the SiC Cascode junction-field-effect transistor (JFET) and Si insulated-gate bipolar transistor (IGBT) were applied to the matrix converter topology. In [5], reliability was analyzed by comparing power loss, thermal performance, and efficiency when a Si IGBT and a gallium nitride (GaN) high-electron mobility transistor (HEMT) were applied to a three-phase inverter. The systems using WBG devices, such as SiC and GaN, achieved a higher efficiency with a lower loss and thermal performance than conventional Si-based systems.

Recently, the results of comparative analyses performed by applying SiC and GaN to the same topology have also been presented [12–17]. In [15], SiC and GaN were applied to an on-board charger to compare power loss, thermal performance, power density, cost, and efficiency. It has been shown

that a higher efficiency and power density can be achieved with GaN than with SiC, as GaN has better physical properties.

Generally, GaN is disadvantageous in that the increase in rate of on-resistance is greater with increasing temperature compared to SiC, and a large gate resistance is required owing to the low threshold voltage and the small range of the gate driving voltage. Additionally, it has a lower thermal conductivity than SiC, and in many cases, a dedicated packaging material, such as GaNPX-4, is used.

SiC has a relatively large parasitic capacitance compared with GaN, which can cause large switching losses. Additionally, because a reverse recovery current exists, the reverse recovery loss may increase at a high switching frequency. However, SiC exhibits superior thermal conductivity to GaN and is applied in a large-area standard package, such as TO-247.

Thus, SiC and GaN exhibit different characteristics. Their device compatibility can vary significantly depending on the operating conditions, such as the voltage, rated power, switching frequency, and thermal management of the system. Therefore, proper device selection requires a device suitability analysis that properly reflects the operating conditions of these systems.

The induction cooker using induction heating (IH) technology is attracting attention as a next-generation heating device to replace the existing stove owing to its high efficiency, safety of heating, and high heating speed. Recently, the output power of such IH systems has been increased by increasing the operating frequency through the development of WBG devices exhibiting small switching loss, in contrast to IGBTs exhibiting large switching loss. Thus, the system size can be reduced while maintaining the output power.

In this study, a SiC MOSFET and a GaN HEMT were applied to the half-bridge resonant converter topology, and their device suitability was analyzed in the IH system. For this purpose, we analyzed the conduction loss of each device considering the junction temperature of the device, the switching loss considering the gate resistance and snubber capacitor, and the reverse conduction loss considering the reverse conduction current. According to the theoretical loss and thermal performance, the suitability of the SiC and GaN devices in the IH system is evaluated. The proposed loss analysis and device suitability analysis are validated by various experimental results based on a constructed half-bridge series resonant converter for a 2-kW IH system using 650-V rated GaN and SiC.

2. IH System with Half-Bridge Converter

2.1. System Description

Figure 1 shows an IH system with a half-bridge converter. Here, V_{DC} represents the input voltage; v_{out} represents the output voltage of the half-bridge; Q_1 and Q_2 represent the top and bottom switches, respectively; C_{S1} and C_{S2} represent snubber capacitors; C_{r1} and C_{r2} represent resonant capacitors. The coil and heating pot can be expressed as an equivalent inductance L_{eq} and equivalent resistance R_{eq} configured in series, as shown in Figure 1. Thus, the operating characteristics are similar to those of normal series resonant converters.

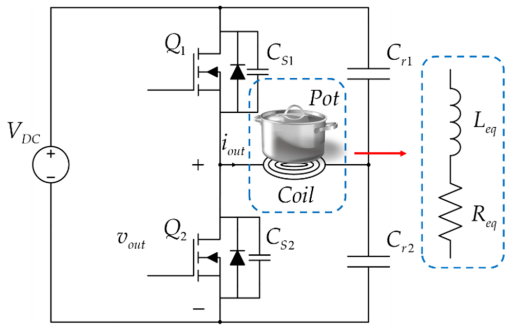

Figure 1. A conventional induction heating (IH) system.

2.2. Characteristics of High-Frequency Operation

In an IH system, the equivalent resistance R_{eq} is mainly increased to increase the output power under limited device performance. There are two methods by which to increase R_{eq} [18]. The first method is to increase the equivalent resistance is by increasing the number of turns in the coils. However, limitations exist with regard to the size of the coils, the wire resistance, and the cost. The second method is to increase the equivalent resistance by increasing the operating frequency, but this presents the limitation of increasing the switching loss. However, small switching losses can be achieved using WBG devices; a higher output power can be achieved by increasing the equivalent resistance without increasing the number of turns of the coil.

Figure 2 shows the equivalent resistance measured using an inductance-capacitance-resistance (LCR) meter according to the number of coil turns and the operating frequency. As shown, the equivalent resistance increased with the number of turns and operating frequency. Upon using the WBG element, it was possible to achieve a high output power in the coil with the same number of turns or to reduce the size of the heat sink or the coil at the same output power, which was advantageous with regard to the overall system size and cost. Therefore, to achieve this advantage using WBG devices, it is necessary to verify the suitability between WBG devices via a comparative analysis of the performance between WBG devices applied to an IH system.

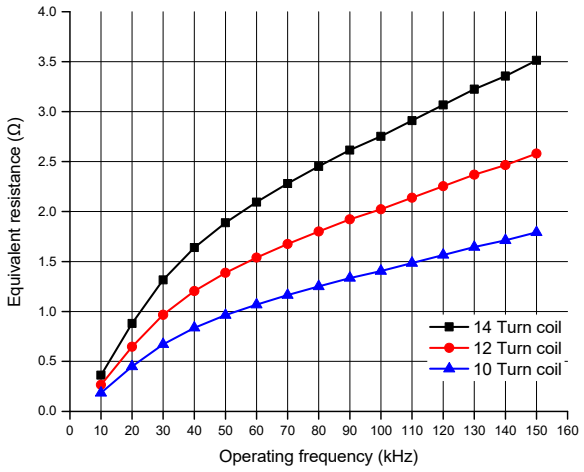

Figure 2. Equivalent resistance according to the number of coil turns and the frequency.

3. Loss Analysis of WBG Device in IH System

In this section, a theoretical loss analysis is performed to compare losses, such as the conduction loss, switching loss, and reverse conduction loss, considering the device characteristics and circuit conditions. The devices used in this study are presented in Table 1.

Table 1. Parameters of the selected devices [19,20].

Parameter	GaN HEMT	SiC MOSFET
Part Number	GS66516T	SCT3030AR
Breakdown Voltage	650 V	650 V
Continuous Current	60 A	70 A

3.1. Conduction Loss Considering Junction Temperature

During operation at the duty ratio $D = 0.5$, the conduction loss for one switching period of a single WBG device considering the dead time is given by (1). Here, T represents the switching period, t_{dead} represents the dead time, and $R_{DS(on)}$ represents the on-resistance. Because $R_{DS(on)}$ varies with

respect to the junction temperature T_j and the gate-source voltage V_{GS}, these parameters should also be considered for accurate conduction-loss analysis.

$$P_{C(Q_1)} = \frac{1}{T}\int_{t_{dead}}^{\frac{T}{2}} R_{DS(on)}\, i_{out}^2\, dt \tag{1}$$

$R_{DS(on)}$ according to the junction temperature can usually be calculated as per presentation in the manufacturer's datasheet. For example, in the case of Rohm's SiC device SCT3030AR, it is assumed that $R_{DS(on)}$ is standard when T_j is 25 °C. As shown in Figure 3, the normalized on-resistance according to T_j can be represented by the change rate ΔR_{T_j}.

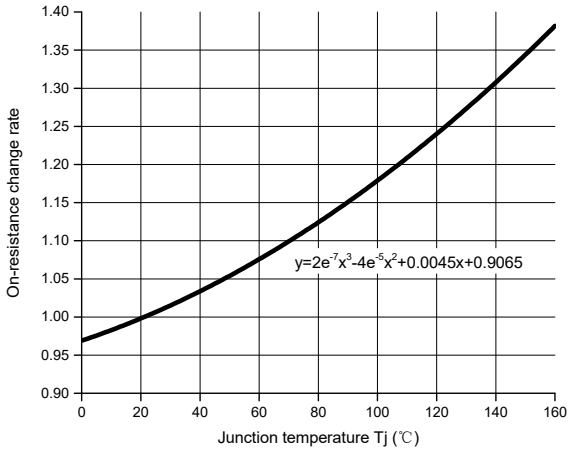

Figure 3. On-resistance change rate according to the junction temperature.

The data in Figure 3 can be represented by (2) through curve-fitting.

$$\Delta R_{T_j} = \left(2\times 10^{-7}\right)T_j^3 - \left(4\times 10^{-5}\right)T_j^2 + 0.0045T_j + 0.9065 \tag{2}$$

Similar to (2), the normalized rate of change according to V_{GS} can also be calculated using the manufacturer's datasheet. The change rate of the on-resistance normalized to 18 V can be expressed as follows:

$$\Delta R_{V_{GS}} = -0.0015V_{GS}^3 + 0.1024V_{GS}^2 - 2.227V_{GS} + 17.684 \tag{3}$$

Finally, the on-resistance $R_{DS(on)}$ considering the junction temperature and gate-source voltage is given as follows:

$$R_{DS(on)} = 0.031 \times \Delta R_{T_j} \times \Delta R_{V_{GS}} \tag{4}$$

The on-resistance for GaN can also be derived from the curve-fitting of the change rate considering the junction temperature and gate-source voltage. The on-resistance equation of GaN device GS66516T is as follows:

$$\Delta R_{T_j} = \left(3\times 10^{-7}\right)T_j^3 - \left(4\times 10^{-5}\right)T_j^2 + 0.0128T_j + 0.7 \tag{5}$$

$$\Delta R_{V_{GS}} = -0.0079V_{GS}^3 + 0.1516V_{GS}^2 - 1.018V_{GS} + 3.3504 \tag{6}$$

$$R_{DS(on)} = 0.025 \times \Delta R_{T_j} \times \Delta R_{V_{GS}} \tag{7}$$

Through the derived equations, the on-resistance according to the junction temperature and gate-source voltage of each device is identical to that in Figure 4. In Figure 4, $R_{DS(on)}$ according to V_{GS} is more sensitive to SiC as V_{GS} decreases. In contrast, $R_{DS(on)}$ increases with T_j for GaN. Therefore, assuming that both devices use the recommended V_{GS}, it is possible to predict that GaN will have a smaller conduction loss under a light load with a lower junction temperature and that as it approaches the rated load, the conduction loss of SiC will decrease.

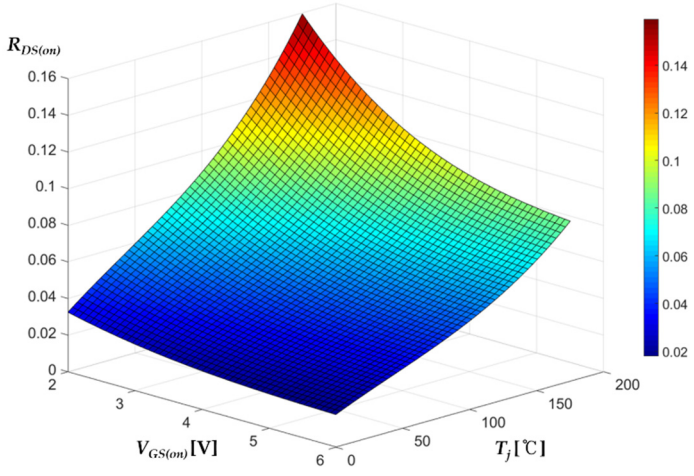

(**a**)

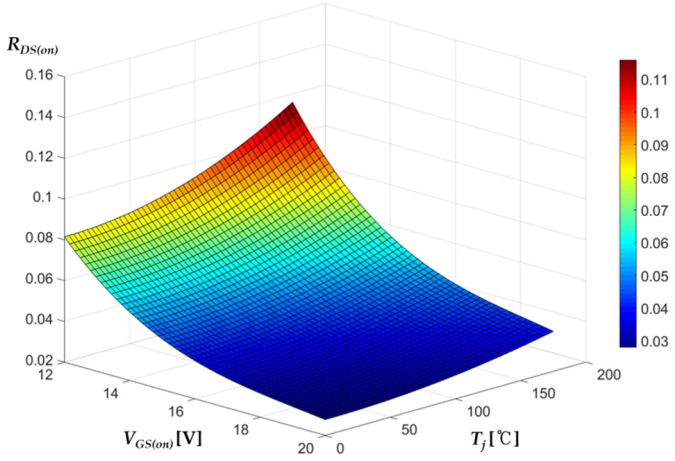

(**b**)

Figure 4. On-resistance according to the junction temperature and gate-source voltage: (**a**) gallium nitride (GaN) high-electron mobility transistor (HEMT); (**b**) silicon carbide (SiC) MOSFET.

3.2. Switching Loss Considering System

The general switching loss P_{sw} is given by (8), where E_{on} represents the switching energy at turn-on, E_{off} represents the switching energy at turn-off, and f_{sw} represents the switching frequency.

$$P_{sw} = \left(E_{on} + E_{off}\right) f_{sw} \tag{8}$$

Typically, turn-on switching losses in IH systems are not theoretically caused by zero voltage switching (ZVS) [21]. Therefore, the losses in the turn-off are compared. To accurately compare the loss, the switching loss equation reflecting the system and device characteristics is derived.

In IH systems, snubber capacitors C_{S1} and C_{S2} are added in parallel with the switch, as shown in Figure 1, to reduce the switching losses during turn-off. This can reduce the switching loss at turn-off by limiting the dv/dt of the drain–source voltage v_{DS} during turn-off switching in ZVS systems. Figure 5 shows the switching turn-off waveform for this IH system. Here, $V_{GS(Drive)}$ represents the gate–source drive voltage, $V_{GS(Plateau)}$ represents the plateau voltage, and $V_{GS(th)}$ represents the threshold voltage. $t_{d,off}$ represents the time from $V_{GS(Drive)}$ to $V_{GS(Plateau)}$, t_{If} represents the time when the i_D current falls, and t_{Vr} represents the time when the v_{DS} voltage increases significantly. V_{DC} represents

the input voltage, I_{off} represents the switch turn-off current, V_1 represents the v_{DS} at time t_3, and V_0 represents the v_{DS} at the beginning of the switch turn-off.

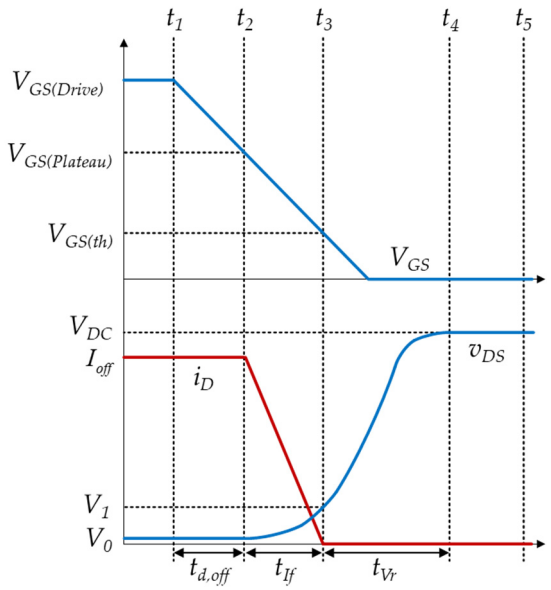

Figure 5. Switch turn-off waveform in the IH system.

In general, turn-off of switching is maintained while the voltage $V_{GS(Plateau)}$ remains constant during the period of the rising v_{DS}; however, in an IH system where a snubber capacitor is added, v_{DS} increases after the switch is turned off. Accordingly, the section maintained at the $V_{GS(plateau)}$ is removed. Consequently, most switching losses occur in the period t_{If} where the current falls. Therefore, the switching-loss equation at t_{If} must be derived.

First, because the i_D current in the t_{If} period is linear, it is derived as in (9). Here, t_2 is assumed to be 0 and i_{C_S} represents the current flowing through the snubber capacitor. As the current i_D decreases, the current for charging and discharging the snubber capacitors at the top and bottom increases.

$$i_D(t) = -\frac{I_{off}}{t_{If}}t + I_{off} = -2i_{C_S} + I_{off} \tag{9}$$

t_{If} can be derived from the discharging of the R-C circuit of the gate resistance and the device input capacitance as follows [22].

$$t_{If} = R_G C_{ISS} \ln\left(\frac{V_{Plateau}}{V_{th}}\right) \tag{10}$$

As indicated by (9), because v_{DS} increases owing to i_{C_S}, it can be expressed by (11), and when it is integrated, it is expressed by (12). Here, V_0 is an initial value, as given by (13).

$$C_S\frac{dv_{DS}}{dt} = i_{C_S} = \frac{1}{2}\cdot\frac{I_{off}}{t_{If}}t \tag{11}$$

$$v_{DS}(t) = V_0 + \frac{I_{off}}{4t_{If}C_S}t^2 \tag{12}$$

$$V_0 = R_{DS(on)}\cdot I_{off} \tag{13}$$

Finally, the E_{off} is derived as

$$E_{off} = \int_0^{t_{If}} v_{DS}(t)\cdot i_D(t)\,dt = -\frac{I_{off}^2 t_{If}^2}{16C_S} + \frac{I_{off}^2 t_{If}^2}{12C_S} - \frac{I_{off}V_0 t_{If}}{2} + I_{off}V_0 t_{If} \tag{14}$$

In (14), t_{If} is the term with the greatest dependence on the device type. Thus, assuming that the same gate resistance is used, GaN with a smaller C_{ISS} is expected to result in a smaller switching loss.

3.3. Reverse Conduction Loss Considering Current

Reverse conduction losses are very important in topologies where ZVS is implemented through the reverse current of a switch, such as a resonant converter. Half-bridge-based IH systems require a comparison of the reverse conduction losses between the two devices, because reverse conduction is performed during dead time to achieve ZVS. The typical reverse conduction loss $P_{C(reverse)}$ in an IH system is given as follows:

$$P_{C(reverse)} = \frac{1}{T}\int_0^{t_{dead}} v_{SD} \cdot |i_{out}|\, dt \tag{15}$$

where v_{SD} represents the source–drain voltage drop for conduction in the reverse direction. To analyze the exact loss, the v_{SD} of each device according to the current can be obtained from the manufacturer's datasheet, and curve-fitting can be used to derive the equation. The v_{SD} for the SiC device is given as follows:

$$v_{SD} = 0.042 \cdot |i_{out}| + 2.14 \tag{16}$$

The v_{SD} of the selected GaN device in this study generally used negative gate voltage $V_{gate\ off}$ at turn-off considering the threshold voltage. It can be expressed by (17) because of the characteristics of the device since a voltage drop of the same magnitude as the negative gate voltage is added at turn-off.

$$v_{SD} = 0.049 \cdot |i_{out}| + 1.74 + V_{gate\ off} \tag{17}$$

However, it is necessary to consider the snubber capacitor because the conduction time changes with the addition of the snubber capacitor, even in the case of reverse conduction loss. The equation for the reverse conduction loss considering the snubber capacitor is as follows. Here, t_5 marks the end of the dead time.

$$P_{C(reverse)} = \frac{1}{T}\int_{t_4}^{t_5} v_{SD} \cdot |i_{out}|\, dt \tag{18}$$

$$t_4 = t_{d,off} + t_{If} + t_{Vr} \tag{19}$$

Because $t_{d,off}$ is the discharging time of an R-C circuit with a gate resistance and device input capacitance, it is derived as follows [22]:

$$t_{d,off} = R_G C_{ISS} \ln\left(\frac{V_{GS(Drive)}}{V_{Plateau}}\right) \tag{20}$$

Because t_{Vr} is determined by the magnitude of the current flowing through the snubber capacitor, it can be derived as shown in (21). V_1 can be calculated by substituting $t = t_{If}$ into (12).

$$t_{Vr} = 2C_S \frac{V_{DC} - V_1}{I_{off}} \tag{21}$$

$$V_1 = V_0 + \frac{I_{off} t_{If}}{4C_S} \tag{22}$$

Assuming that both devices use a gate voltage of zero at turn-off, a v_{SD} with slightly smaller GaN appears at currents of < 50 A. However, in contrast to SiC devices with a threshold voltage of approximately 4 V, GaN devices exhibit a low threshold voltage of 1 V; thus, if the negative voltage is used to increase the resistance to noise, the v_{SD} increases by the magnitude of the negative voltage, as indicated by (17). Hence, it is expected that smaller reverse conduction losses occur in SiC.

4. Device Suitability Analysis in IH System

The circuit conditions for the device comparisons of the power loss and thermal performance are presented in Table 2.

Table 2. Value of circuit components.

Component	Value
Input Voltage V_{DC}	260 V
Equivalent Inductance L_{eq}	18.40 μH
Equivalent Resistance R_{eq}	5.16 Ω
Resonant Capacitance C_{r1} C_{r2}	0.068 μF
Snubber Capacitance C_{s1} C_{s2}	10 nF
Rated Power	2 kW
Dead Time t_{dead}	500 ns
Total Gate Resistance R_G	7 Ω

4.1. Power Loss

According to the loss model derived in Section 3, the power losses were compared by calculating the theoretical conduction losses, switching losses, and reverse conduction losses. It was assumed that the junction temperature was set as 40 °C at 800 W and increased by 10 °C each time the power increased by 200 W. The recommended V_{GS} values for the SiC and GaN devices are 18 and 6 V, respectively. Negative voltages are recommended because the GaN's low threshold voltage can cause false turn-on at turn-off. Accordingly, the calculation was performed with voltages of 0 V for SiC and −3 V for GaN.

Figure 6 shows the loss breakdown based on the output power calculated according to the assumption. As shown in Figure 6, in GaN, the conduction losses were smaller for lighter loads. As the output power increased, less conduction loss was observed in SiC, where the increase in on-resistance with respect to the temperature was relatively small. This is because the temperature was assumed to increase by 10 °C for increments of 200 W.

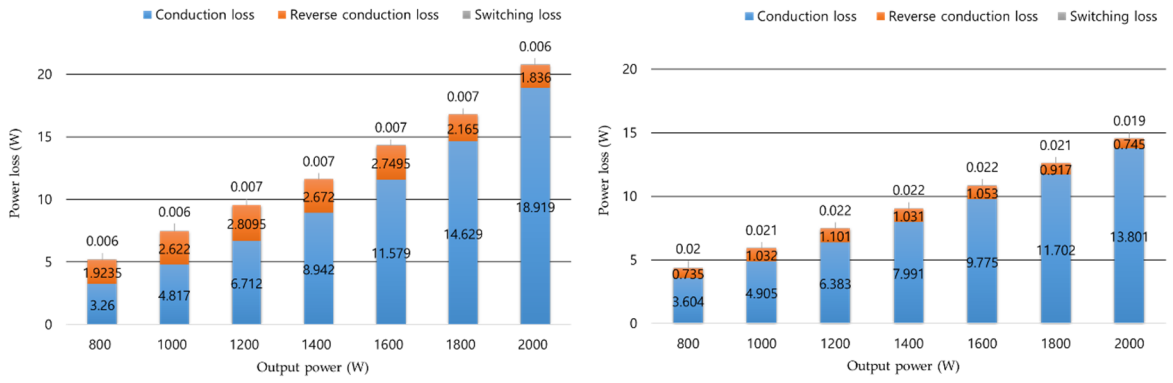

(**a**) (**b**)

Figure 6. Loss breakdown according to the output power: (**a**) GaN HEMT; (**b**) SiC MOSFET.

The switching losses were very small for both devices when snubber capacitors were added. GaN exhibited smaller losses because of the low parasitic capacitance.

The reverse conduction loss was small because the reverse conduction time during the dead time was significantly reduced when the snubber capacitor was added. As shown in (17), GaN's v_{SD} exhibited a relatively large loss compared with SiC's v_{SD} when the voltage drop occurred, owing to the addition of $V_{gate\ off}$.

4.2. Thermal Performance

Thermal performance is an important factor in determining system size and cost. On comparing the thermal performances of the GaN and SiC devices, a lower thermal performance at the same losses increases the size and cost of the system, which can result in an inability to achieve rated loads or requirement of larger heat sinks. Therefore, it is necessary to compare the thermal performances of devices via thermal analysis simulations and experiments.

A thermal analysis model was developed that reflected the packaging and physical properties of each device, and the same fan and heat sink were applied to conduct a simulation. Figure 7 shows the results of the thermal analysis simulations where a loss of 30 W occurred in each device.

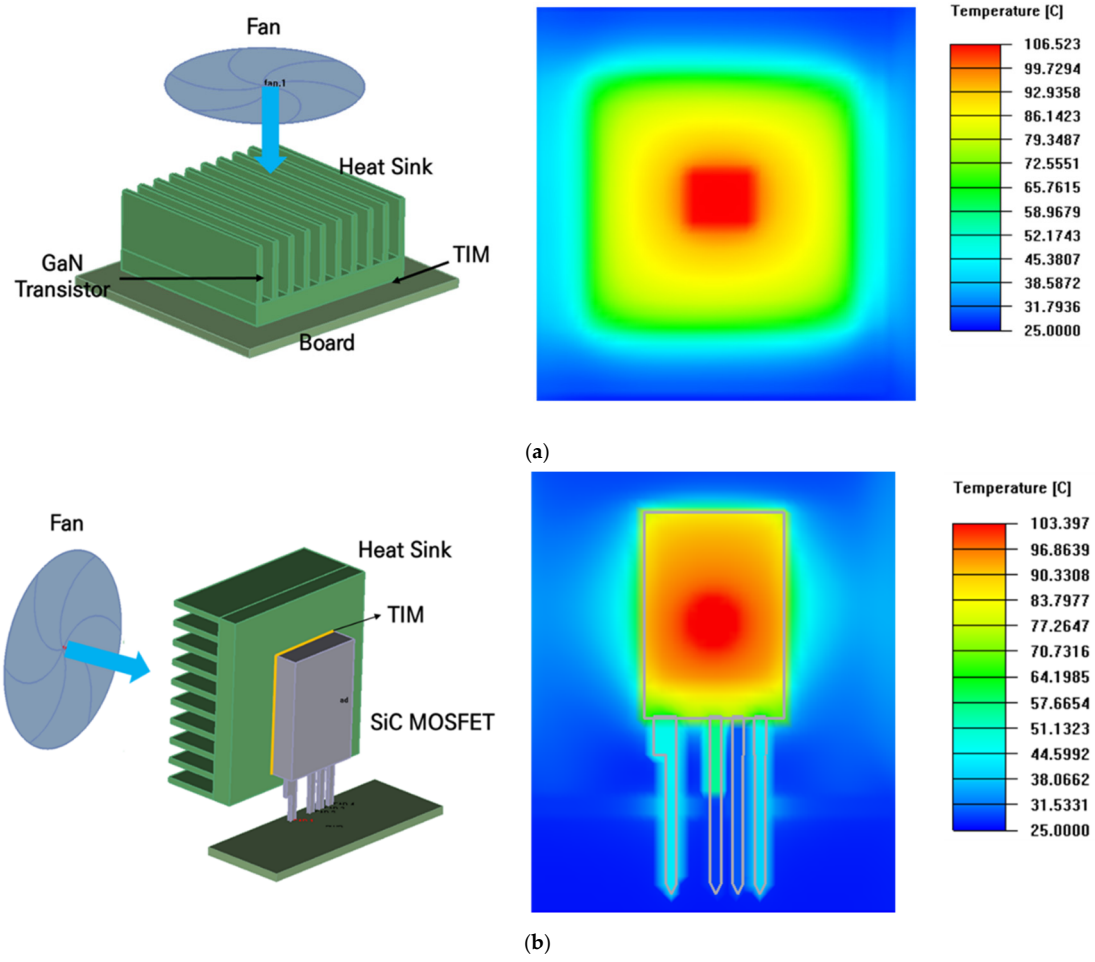

Figure 7. Thermal analysis simulation results: (**a**) GaN HEMT; (**b**) SiC MOSFET.

In Figure 7, the maximum value represents the junction temperature, with different results observed for the same heat-dissipation conditions and losses. This is expected to be a result of the differences in the physical properties of the devices and the difference in the thermal resistance owing to the packaging. In order to improve the thermal performance of the device, it is necessary to consider the location and direction of the fan for cooling the heat sink, the air flow value, and the selection of a thermal interface material (TIM) with low thermal resistance.

4.3. Cost

Table 3 shows the cost comparison result based on the experimental set consisting of SiC and GaN. The comparison components include the converter used as the gate power source, the gate driver, the main switch, the snubber capacitor, the resonant capacitor, the working coil, and the total cost of

the system. The DC-DC converter has a higher cost with SiC, and the gate driver has a similar cost. The cost of the main switch is relatively high with GaN compared to SiC, and other elements use the same parts so it does not affect the cost. The total cost is higher in the GaN board, which is a result of the relatively high cost difference of the main switch.

Table 3. Comparison of system components.

Component	Comparison
DC-DC Converter	GaN < SiC
Gate Driver	GaN ≅ SiC
Main Switch	GaN > SiC
Snubber Capacitor	GaN = SiC
Resonant Capacitor	GaN = SiC
Working Coil	GaN = SiC
Total Cost	GaN > SiC

5. Experimental Comparative Analysis and Verification

The experimental setup was constructed as shown in Figure 8 to conduct the experimental comparative analysis and verification. The circuit conditions of the IH system used in the experiment are presented in Table 2.

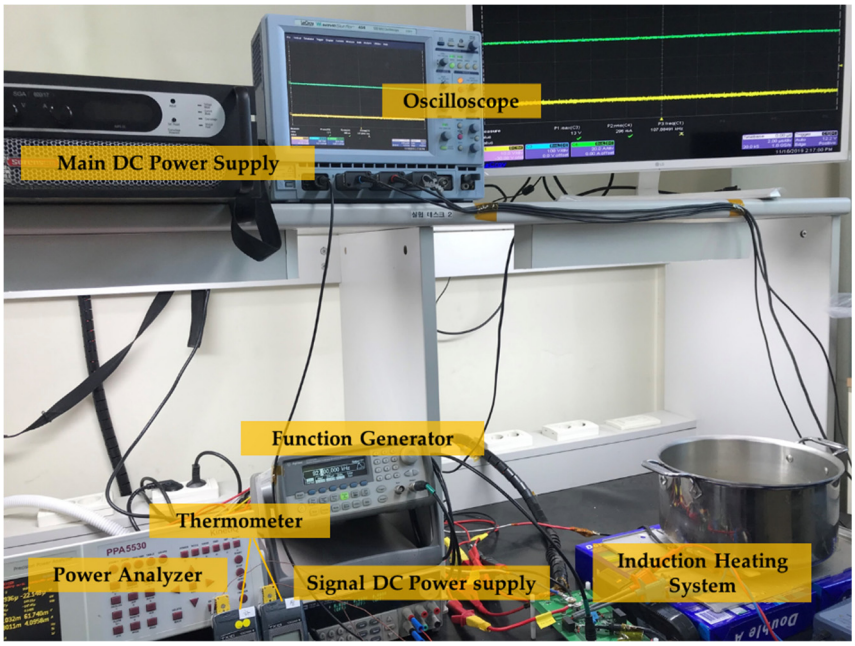

Figure 8. IH system experiment configuration.

5.1. Power Loss

An efficiency measurement experiment was conducted for loss analysis. Figure 9 shows experimental waveforms for each device at a rated load of 2 kW. The drain–source voltage and gate–source voltage of the half-bridge top switch Q_1, as well as the output current i_{out}, were measured.

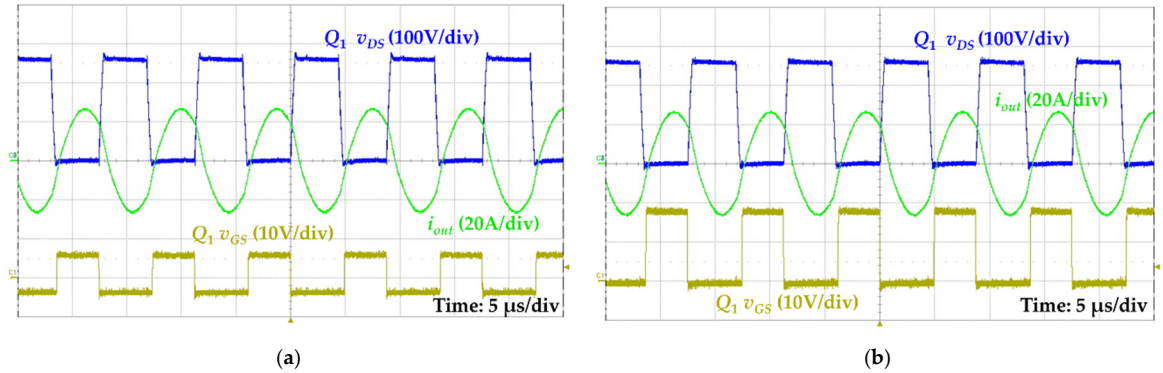

(**a**) (**b**)

Figure 9. Experimental waveform at 2 kW: (**a**) GaN HEMT; (**b**) SiC MOSFET.

As shown in Figure 9, ZVS was performed because zero voltage was achieved before both devices were turned on. The v_{DS} exhibited greater overshoot and undershoot in the experimental waveform of GaN than in that of SiC. This is because when driving GaN, a negative voltage with a magnitude of 3 V was used to prevent false turn-on, resulting in a large reverse conduction voltage drop.

Figure 10 shows the loss breakdown results estimated from the experimental data. The junction temperature was estimated by applying thermal analysis simulations to the total losses measured by the power analyzer at 2 kW. Accordingly, the conduction loss was calculated. The reverse conduction loss was calculated to reflect the reverse conduction time determined using the experimental waveform. Losses apart from these were assumed to be switching losses.

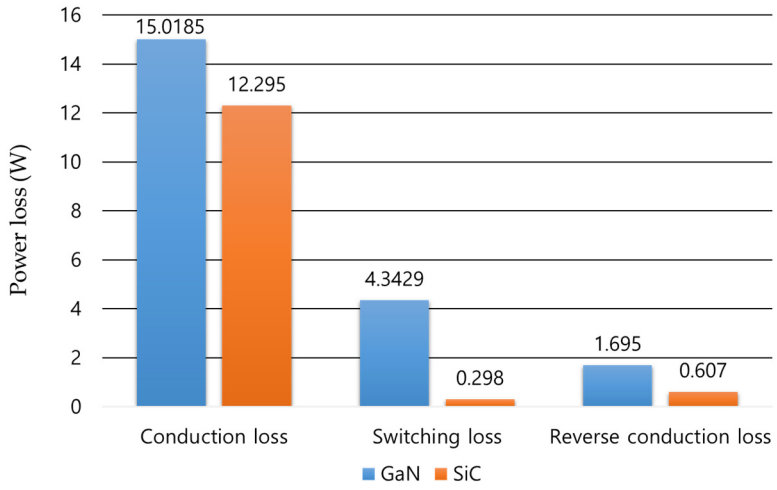

Figure 10. Loss breakdown reflecting experimental values at 2 kW.

As shown in Figure 10, since the on-resistance of GaN increases as junction temperature increases, compared to SiC, the conduction loss of GaN is greater. This is similar to the theoretical result. Regarding switching losses, GaN theoretically exhibited a lower loss than SiC; however, it actually exhibited larger experimental losses. This was the result of the ringing of parasitics becoming more dominant because the switching losses in t_{If} were very small, as dv/dt was limited by the snubber capacitor. In the case of GaN, when the same gate resistance was used, the di/dt of the switch was very large owing to the low parasitic capacitance. Therefore, the loss due to ringing was expected to be greater than that for SiC. Reverse conduction losses resulted in larger losses in GaN, similar to the theoretical estimates. Finally, the efficiency according to the measured load is shown in Figure 11. Here, the conditions of the simulation were identical to those in Table 2.

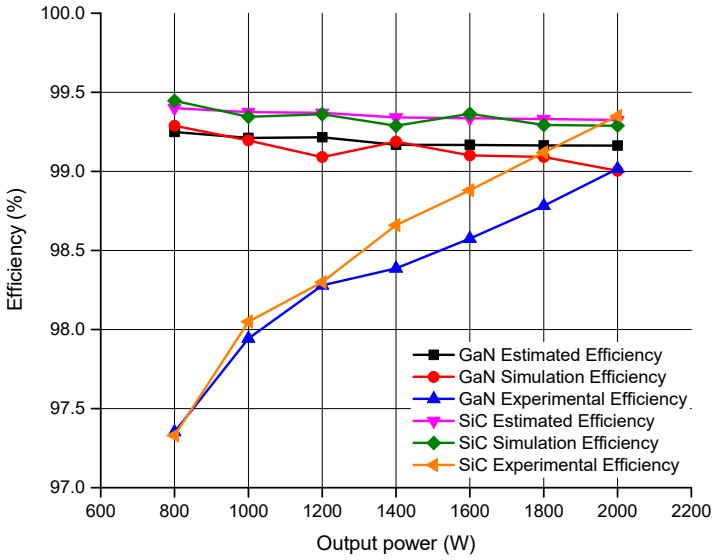

Figure 11. Efficiency according to the output power.

As shown in Figure 11, SiC exhibited a higher efficiency than GaN at most of the efficiencies, as estimated in Section 4. As the output power decreased, the junction temperature of the device decreased; thus, the on-resistance of the GaN device was lower than that of the SiC one, and the conduction loss of the GaN device was smaller than that of the SiC one under a light load. Consequently, as the load decreased, the difference in efficiency between the two devices gradually decreased. Additionally, the predictive efficiency, simulation efficiency, and experimental efficiency at the rated load were very similar, confirming that the loss modeling of the device was executed well.

However, in contrast to the predicted and simulated values, the experimental efficiency decreased with light loads, for both GaN and SiC. The dominant cause is predicted to be the influence of parasitic components, such as parasitic inductance and parasitic resistance. The IH system operates at a higher switching frequency under light load, and as the switching frequency increases, the influence of parasitic components increases. Accordingly, the error rate increases at light load. In order to estimate the efficiency more accurately, it is necessary to study a model that sufficiently considers parasitic components.

5.2. Thermal Performance

Figure 12 shows the experimental results for the device package temperature according to the output power. The results in Figure 12 differ depending on the devices, similar to Figure 7. As mentioned previously, this can be interpreted as the influence of the physical properties and packaging of the device. In particular, the difference was similar to that shown in Figure 7 when the experimental efficiencies of the two devices were compared at similar power levels of 800 W.

As shown in Figures 11 and 12, the difference in efficiency between GaN and SiC is relatively small at 800 W, where the device temperature is low. However, as the temperature increases, the most dominant conduction loss occurs in GaN rather than SiC, and it can be seen that the difference in efficiency gradually increases.

Figure 13 is the finite element method (FEM) result applying the experimental loss at 2 kW. In Figure 13, (a) represents the package temperature of GaN, (b) represents the junction temperature of GaN, (c) represents the package temperature of SiC, and (d) represents the junction temperature of SiC. The reliability of the temperature analysis model was verified by the similarity between the measured results at 2 kW of Figure 12 and the temperature of the FEM analysis in Figure 13.

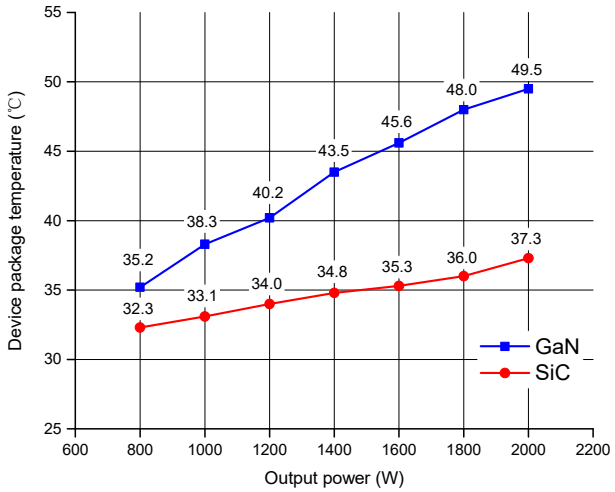

Figure 12. Device package temperature measurement results according to the output power.

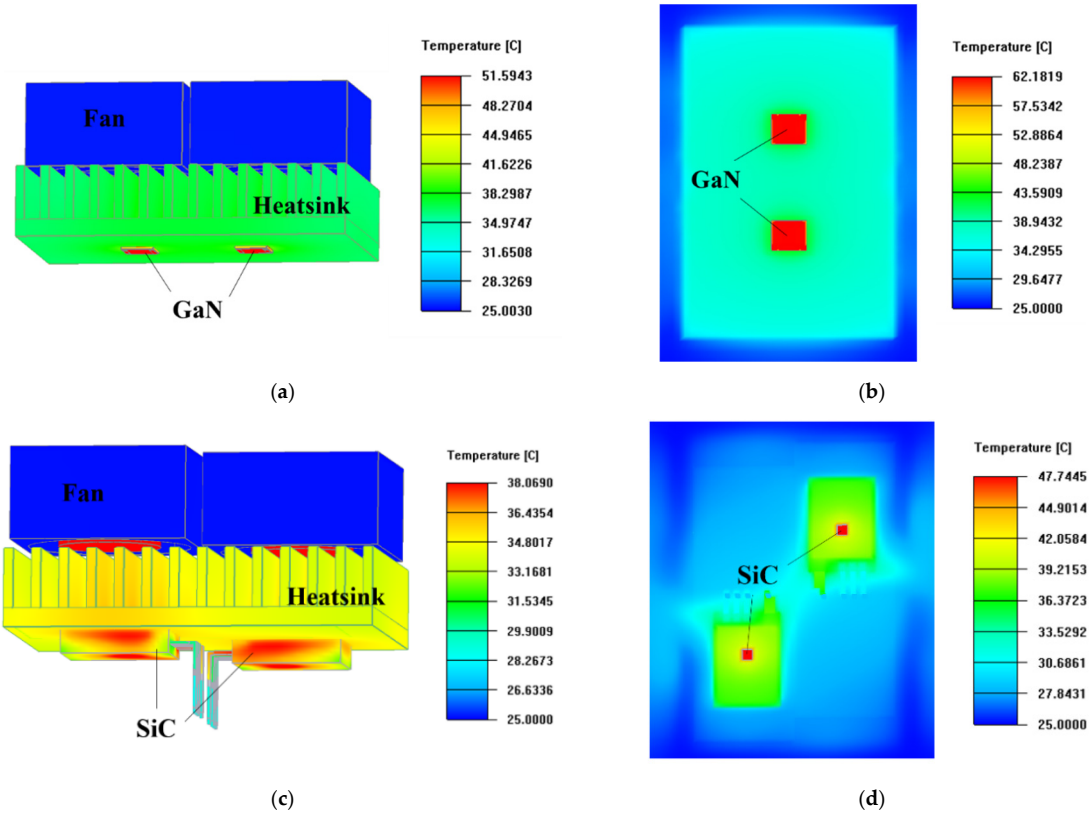

Figure 13. FEM analysis result with experimental loss: (**a**) GaN HEMT package temperature; (**b**) GaN HEMT junction temperature; (**c**) SiC MOSFET package temperature; (**d**) SiC MOSFET junction temperature.

6. Conclusions

Device suitability in an IH system was analyzed by comparing the performance of GaN and SiC represented by WBG devices. Loss modeling was performed, considering the junction temperature, gate–source voltage, gate resistance, gate voltage, and snubber capacitor for each device. Additionally, a thermal analysis model was developed according to the device's physical properties and packaging. Using the model, the device suitability was analyzed via comparative power-loss calculations and thermal performance simulations. The loss in the IH systems in the 100-kHz band was dominated using

conduction losses and reverse conduction losses, as switching losses were reduced owing to the snubber capacitors. Thus, SiC exhibited a higher efficiency than GaN as the load increased for the selected devices. Regarding the thermal performance, different results were observed for the same losses owing to differences in the thermal conductivity and packaging, and 2-kW prototype converters using GaN and SiC were built. The loss and thermal performance were experimentally compared, and the theoretical loss and thermal analysis model was validated. However, due to parasitic components, the error rate of efficiency tended to increase with light load. In order to accurately estimate these efficiencies, a study of a theoretical model that fully considers parasitic components is needed in the future.

Author Contributions: Conceptualization, K.-H.C. and R.-Y.K.; Formal analysis, K.-H.C.; Project administration, R.-Y.K.; Supervision, R.-Y.K.; Validation, K.-H.C. and C.-T.J.; Visualization, K.-H.C. and R.-Y.K.; Writing—original draft, K.-H.C.; Writing—review and editing, K.-H.C., C.-T.J. and R.-Y.K. All authors have read and agreed to the published version of the manuscript.

Funding: This work was supported by "Human Resources Program in Energy Technology" of the Korea Institute of Energy Technology Evaluation and Planning (KETEP), granted financial resources from the Ministry of Trade, Industry and Energy, Republic of Korea (No. 2018201010650A, No. 20184010201710).

Conflicts of Interest: The authors declare no conflict of interest.

References

1. Domes, D.; Hofmann, W.; Lutz, J. A first loss evaluation using a vertical SiC-JFET and a conventional Si-IGBT in the bidirectional matrix converter switch topology. In Proceedings of the European Conference on Power Electronics and Application, Dresden, Germany, 11–14 September 2005; pp. 3–10.
2. Gao, Y.; Huang, A.; Krishnaswami, S.; Richmond, J.; Agarwal, A. Comparison of static and switching characteristics of 1200 V 4H-SiC BJT and 1200 V Si-IGBT. *IEEE Trans. Ind. Appl.* **2008**, *44*, 887–893. [CrossRef]
3. Biela, J.; Schweizer, M.; Waffler, S.; Kolar, J.W. SiC versus Si-evaluation of potentials for performance improvement of inverter and DC-DC converter system by SiC power semiconductors. *IEEE Trans. Ind. Electron.* **2011**, *58*, 2872–2882. [CrossRef]
4. Zapico, A.; Gabiola, I.; Apinaniz, S.; Santiago, F.; Pujana, A.; Rodriguez, A.; Briz, F. SiC and Si transistors comparison in boost converter. In Proceedings of the International Power Electronics and Motion Control Conference (EPE/PEMC), Novi Sad, Serbia, 4–6 September 2012; pp. 1–6.
5. Shirabe, K.; Swamy, M.; Kang, J.K.; Hisatsune, M.; Wu, Y.; Kebort, D.; Honea, J. Efficiency comparison between Si-IGBT-based drive and GaN-based drive. *IEEE Trans. Ind. Appl.* **2014**, *50*, 566–572. [CrossRef]
6. Tuysuz, A.; Bosshard, R.; Kolar, J.W. Performance comparison of a GaN GIT and a Si IGBT for high-speed drive applications. In Proceedings of the International Power Electronics Conference (ECCE ASIA), Hiroshima, Japan, 18–21 May 2014; pp. 1904–1911.
7. Leon-Masich, A.; Blavi-Valderrama, H.; Bosque-Moncusi, J.M.; Martinez-Salamero, L. Efficiency comp-arison between Si and SiC-based implementations in a high gain DC-DC boost converter. *IET Power Electron.* **2015**, *8*, 869–878. [CrossRef]
8. Swamy, M.; Kang, J.K.; Shirabe, K. Power loss, system efficiency, and leakage current comparison between Si IGBT VFD and SiC FET VFD with various filtering options. *IEEE Trans. Ind. Appl.* **2015**, *51*, 3858–3866. [CrossRef]
9. Gurpinar, E.; Yang, Y.; Iannuzzo, F.; Castellazzi, A.; Blaabjerg, F. Reliability-driven assessment of GaN HEMTs and Si IGBTs in 3L-ANPC PV inverters. *IEEE J. Emerg. Sel. Topics Power Electron.* **2016**, *4*, 956–969. [CrossRef]
10. Duarte, R.R.; Ferreira, G.F.; Dalla-Costa, M.A.; Alonso, J.M. Performance comparison of Si and GaN transistors in a family of synchronous buck converters for LED lighting applications. In Proceedings of the IEEE Industry Applications Society Annual Meeting, Portland, OR, USA, 2–6 October 2016; pp. 1–7.
11. Acharya, S.; She, X.; Datta, R.; Todorovic, M.H.; Mandrusiak, G. Comparison of 1.7kV 450A SiC-MOSFET and Si-IGBT based modular three phase power block. In Proceedings of the IEEE Energy Conversion (ECCE), Cincinnati, OH, USA, 1–5 October 2017; pp. 5119–5125.
12. Choi, J.W.; Tsukiyama, D.; Rivas, J. Comparison of SiC and eGaN devices in a 6.78 Mhz 2.2 kW resonant inverter for wireless power transfer. In Proceedings of the IEEE Energy Conversion (ECCE), Milwaukee, WI, USA, 18–22 September 2016.

13. Gurpinar, E.; Castellazzi, A. Single-phase T-type inverter performance benchmark using Si IGBTs, SiC MOSFETs, and GaN HEMTs. *IEEE Trans. Power Electron.* **2016**, *31*, 7148–7160. [CrossRef]
14. Liu, Y.; Ge, B.; Abu-Rub, H.; Zhang, H.; Balog, R.S. Comparison of SiC and GaN devices for front-end isolation of quasi-Z-source cascaded multilevel photovoltaic inverter. In Proceedings of the IEEE Energy Conversion (ECCE), Milwaukee, WI, USA, 18–22 September 2016.
15. Taylor, A.; Lu, J.; Zhu, L.; Bai, K.H.; McAmmond, M.; Brown, A. Comparison of SiC MOSFET-based and GaN HEMT-based high-efficiency high-power-density 7.2 kW EV battery chargers. *IET Power Electron.* **2018**, *11*, 1849–1857. [CrossRef]
16. Abdelrahman, A.S.; Erdem, Z.; Attia, Y.; Youssef, M.Z. Wide bandgap devices in electric vehicle converters: A performance survey. *Can. J. Elect. Comput. E* **2018**, *41*, 45–54.
17. Su, G.J. Comparison of Si, SiC, and GaN based isolation converters for onboard charger applications. In Proceedings of the IEEE Energy Conversion (ECCE), Portland, OR, USA, 23–27 September 2018; pp. 1233–1239.
18. Tanaka, T. A new induction cooking range for heating any kind of metal vessels. *IEEE Trans. Consum. Electron.* **1989**, *35*, 635–641. [CrossRef]
19. GaN Systems, GS66516T DATA SHEET. Available online: https://gansystems.com/wp-content/uploads/2020/04/GS66516T-DS-Rev-200402.pdf (accessed on 2 April 2020).
20. ROHM Semiconductor, SCT3030AR DATA SHEET. Available online: https://fscdn.rohm.com/en/products/databook/datasheet/discrete/sic/mosfet/sct3030ar-e.pdf (accessed on 31 July 2019).
21. Kazimierczuk, M.K. Class D voltage-switching MOSFET power amplifier. *IEE Electric. Power. Appl.* **1991**, *138*, 285–296. [CrossRef]
22. Chen, Z. Characterization and Modeling of High-Switching-Speed Behavior of SiC Active Devices. Master's Thesis, Virginia Polytechnic Institute and State University, Blacksburg, VA, USA, December 2009.